

Electronic Supplementary Information

Tuning properties of CoFe-layered double hydroxide by vanadium substitution for improved water splitting activity

Baghendra Singh and Arindam Indra*

Department of Chemistry, Indian Institute of Technology (BHU), Varanasi, Uttar Pradesh-221005

(India)

E-mail: arindam.chy@iitbhu.ac.in

1. CHEMICALS

The chemicals were purchased from Sigma-Aldrich and Alfa Aesar and used without any further purification. Carbon cloth was procured from Nara Cell-Tech, Seoul, Korea. Double distilled water was used for the experiments and electrochemical measurements.

2. INSTRUMENTS

The powder X-ray diffraction patterns of the synthesized materials have been recorded in a Rigaku SmartLab 9 kW powder X-Ray diffractometer using Cu K_α radiation ($\lambda=1.5418 \text{ \AA}$). Fourier transformed-infrared (FT-IR) spectroscopy has been performed using Thermo Scientific Nicolet iS5 spectrometer with ATR mode. Raman spectroscopic studies have been performed by utilizing STR 300 spectrometer. Energy-dispersive X-ray studies have been carried out by 51N1000-EDS system. The X-ray photoelectron spectra have been recorded using VG/VG ESCA LAB 220i and Thermo Avantage software was used for the data analysis. SEM studies have been carried out by field emission scanning electron microscope EVO-Scanning Electron Microscope MA15/18. Transmission electron microscopic (TEM) studies have been performed by using a Tecnai G2 20 TWIN transmission electron microscope. TEAM EDS SYSTEM with octane plus SDD detector has been utilized for elemental mapping. Atomic force microscopic studies have been performed by NTEGRA Prima. The electrochemical measurements have been carried out in Autolab potentiostat/galvanostat (Model PGSTAT-72637).

3. ELECTROCHEMICAL CHARACTERIZATIONS

1.0 M aqueous KOH solution was used to investigate water oxidation activity in a single-compartment three-electrode electrochemical cell (catalyst@CC as a working electrode, Pt wire as a counter electrode, and Ag/AgCl as a reference electrode). Cyclic voltammetric (CV) and linear sweep voltammetric (LSV) profiles were corrected for *iR* drop (80%) and background current. The current density is normalized against the catalyst loading (mg) and compared to assess the electrochemical performance. Electrochemical impedance spectroscopic (EIS) measurements were carried out in the frequency range from 0.1 to 100,000 Hz and amplitude of 5 mV. Chronoamperometric measurements have been carried out for 24 h at a constant anodic or cathodic potential.

Table S1

Catalysts	Initial mmol of metals			V (%)	Total (mmol)	Catalyst loading (mg)
	Co (mmol)	Fe (mmol)	V (mmol)			
CoFe-LDH	1.0	1.0	0.0	0.0	2.0	2.4 ± 0.1
V_{0.1}-CoFe-LDH	0.9	0.9	0.2	10	2.0	2.3 ± 0.1
V_{0.2}-CoFe-LDH	0.8	0.8	0.4	20	2.0	2.4 ± 0.2
V_{0.3}-CoFe-LDH	0.7	0.7	0.6	30	2.0	2.5 ± 0.2
V_{0.5}-CoFe-LDH	0.5	0.5	1	50	2.0	2.3 ± 0.1

4. FIGURES

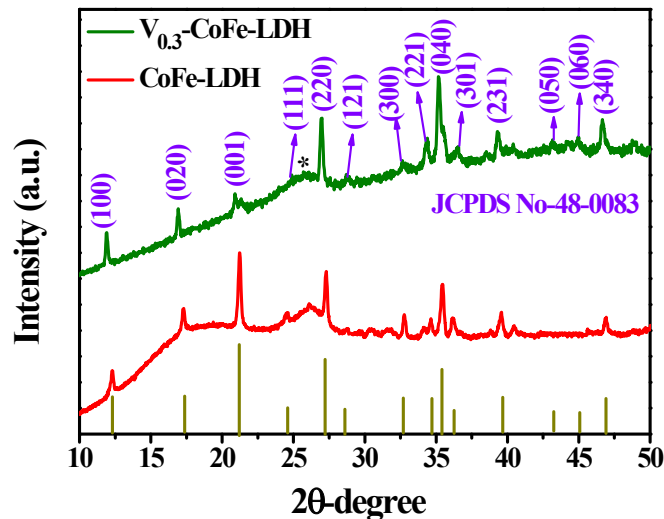


Figure S1. Powder X-ray diffraction (PXRD) pattern of $V_{0.3}$ -CoFe-LDH was compared with CoFe-LDH. The peaks were indexed for layered double hydroxide structure on carbon cloth. The diffraction peaks at 11.9° , 21.2° , 35.2° , 39.2° , and 46.6° were indexed for the (100), (020), (040), (231), and (340) facets of $V_{0.3}$ -CoFe-LDH. The peaks corresponding to the (100) and (001) planes of $V_{0.3}$ -CoFe-LDH shifted to lower 2θ values (0.39° and 0.31° , respectively) compared to CoFe-LDH. Therefore, the d-spacing values for the (100) and (001) reflections were increased (0.74 nm and 0.42 nm, respectively) after vanadium substitution in CoFe-LDH [$d(100) = 0.72$ nm and $d(001) = 0.41$ nm].^[S1-S2]

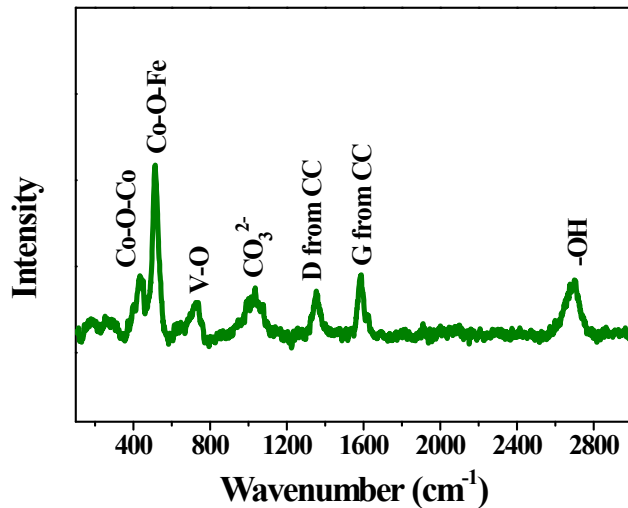


Figure S2. Raman spectrum of $V_{0.3}$ -CoFe-LDH representing the peaks at 435 cm^{-1} and 508 cm^{-1} for the Co-O-Co and Co-O-Fe vibrations, respectively. The peak at 730 cm^{-1} was attributed to the V-O vibration, whereas the peak at 1020 cm^{-1} was originated from intercalated carbonate ions. The peaks at 1355 cm^{-1} and 1580 cm^{-1} were originated from D and G band stretching of carbon cloth while the peak at 2697 cm^{-1} was assigned for hydrogen bonded –OH group.^[S3-S6]

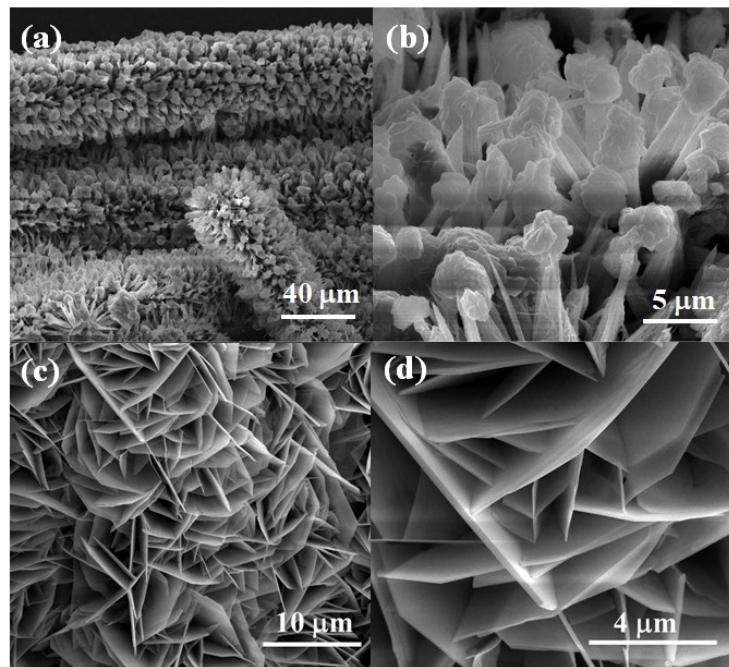


Figure S3. (a-b) Scanning electron microscopic (SEM) images of $\text{V}_{0.3}\text{-CoFe-LDH}$ catalyst showing the nanosheets stacked with each other to form flower-like morphology and (c-d) SEM images of CoFe-LDH indicating the nanosheet morphology.

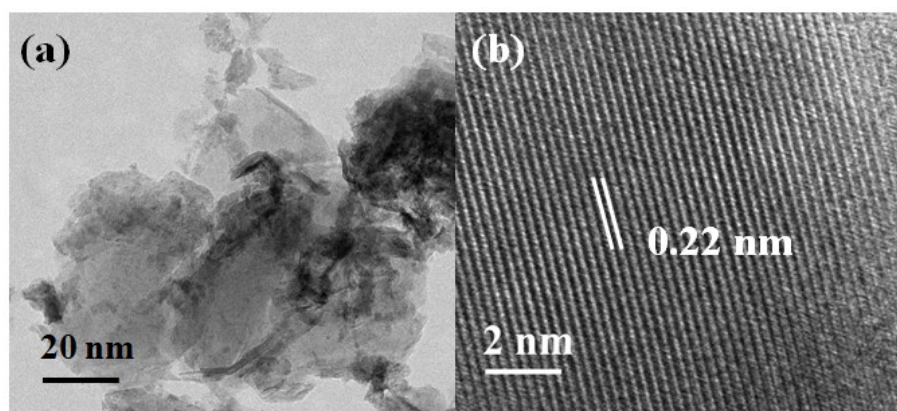


Figure S4. (a) Transmission electron microscopic (TEM) image of CoFe-LDH catalyst confirming the transparent ultrathin nanosheet morphology and (b) High-resolution transmission electron microscopic (HRTEM) image showing the lattice spacing of 0.22 nm corresponding to (231) plane for CoFe-LDH [JCPDS No-48-0083].^[S7]

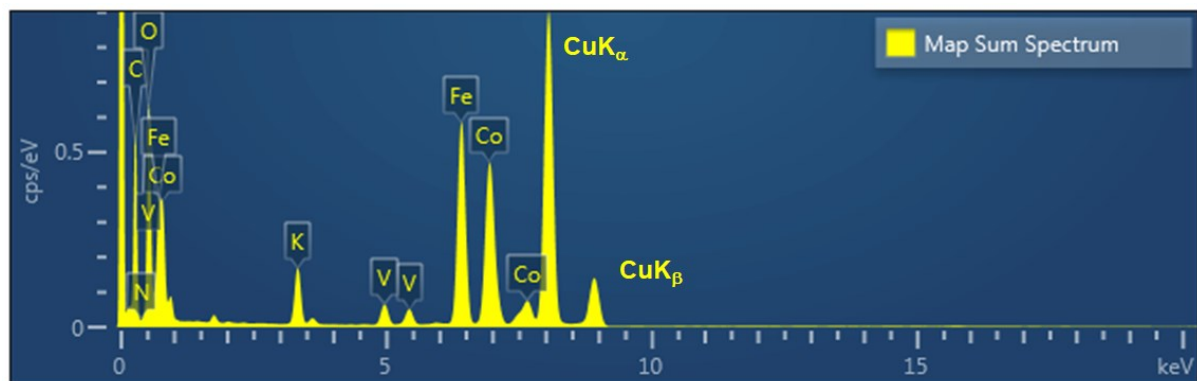


Figure S5. Energy dispersive X-ray (EDX) spectrum of $V_{0.3}$ -CoFe-LDH showing the presence of Co, Fe, and V in the catalyst. The peaks of CuK_{α} and CuK_{β} were originated from TEM grid.

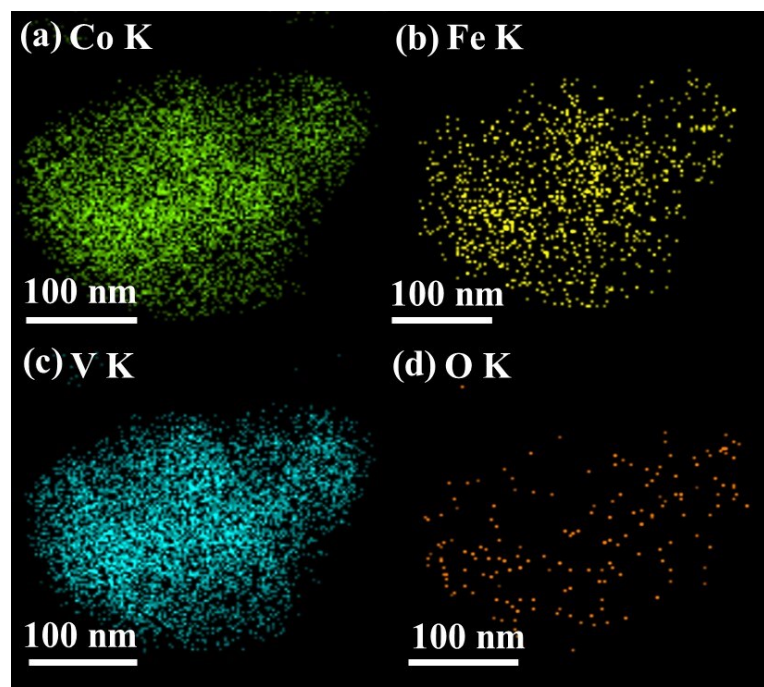


Figure S6. Elemental mapping of $V_{0.3}$ -CoFe-LDH showing the uniform distribution of Co, Fe, V, and O.

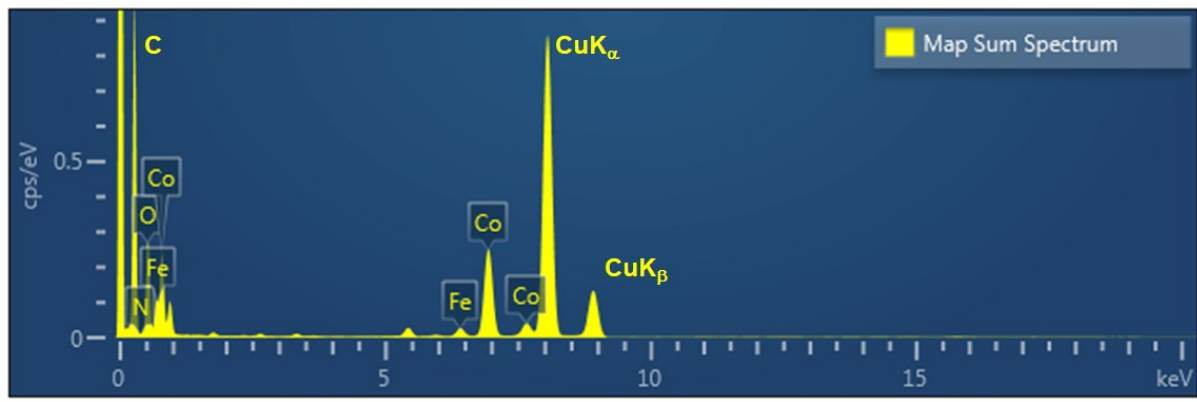


Figure S7. Energy dispersive X-ray (EDX) spectrum of CoFe-LDH catalyst showing the presence of Co and Fe. The peaks of CuK α and CuK β were originated from TEM grid.

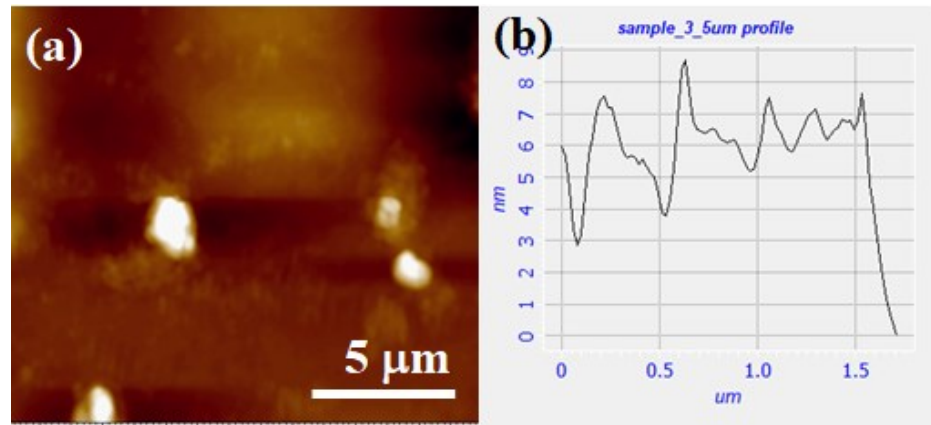


Figure S8. (a) Atomic force microscopic (AFM) image of V_{0.3}-CoFe-LDH and (b) corresponding height profile confirming the 6-8 nm thickness of the nanosheets.

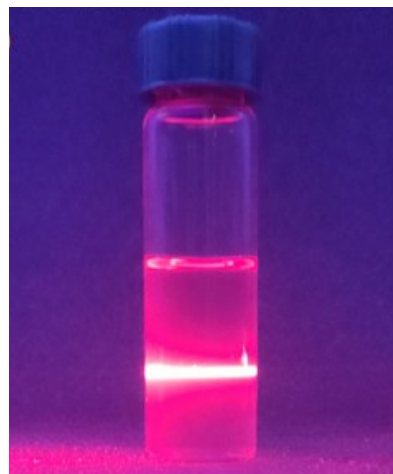


Figure S9. Tyndall effect under a laser beam irradiation indicated the uniform dispersion V_{0.3}-CoFe-LDH because of atomic level thickness.

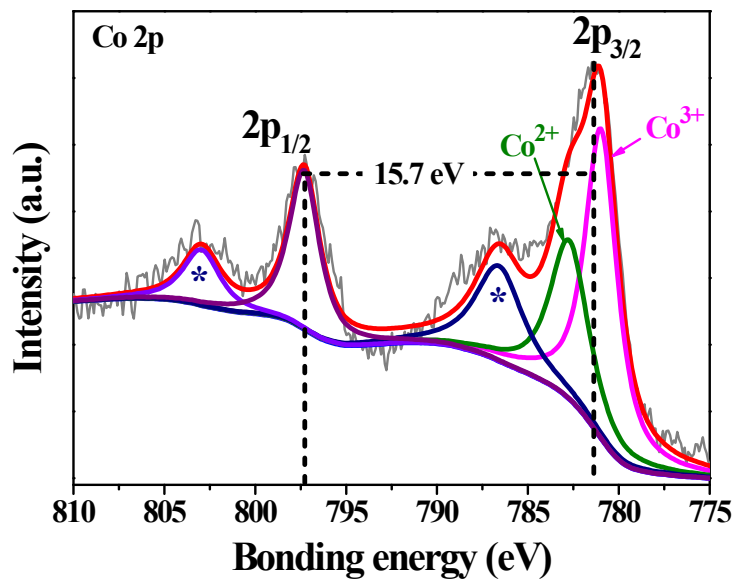


Figure S10. Co 2p XP-spectrum of V_{0.3}-CoFe-LDH was fitted into two peaks at binding energies 781.3 eV and 797.1 eV for 2p_{3/2} and 2p_{1/2}, respectively. The 2p_{3/2} peak was deconvoluted for Co³⁺ at 781.0 eV and Co²⁺ at 782.8 eV. The peak at 786.7 eV was attributed to the satellite peak of Co²⁺. The spin-orbit coupling spacing was calculated to be 15.7 eV indicating the presence of Co²⁺ as the major species.^[S1,S8-S12]

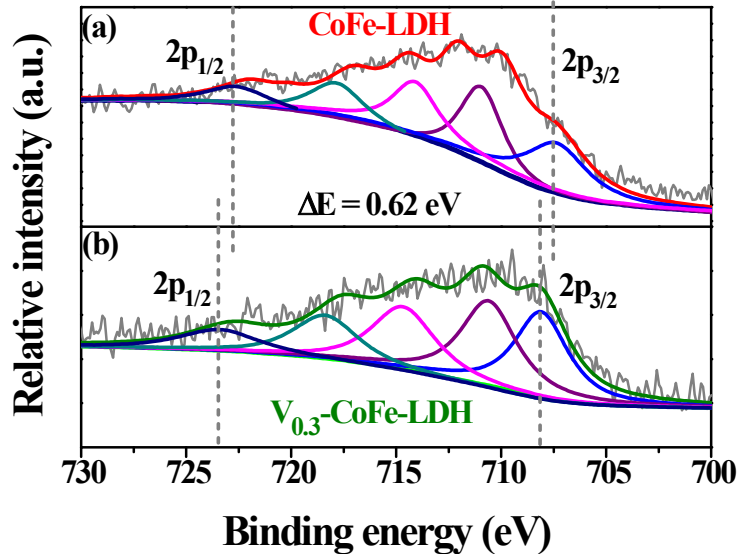


Figure S11. (a) Fe 2p XP-spectrum of CoFe-LDH was fitted into two peaks for 2p_{3/2} (707.5 eV) and 2p_{1/2} (722.9 eV). The peaks at 707.5 eV and 711.0 eV were assigned for Fe²⁺ and Fe³⁺ while the peaks at 714.2 eV and 718.0 eV were attributed to the satellites of Fe²⁺ and Fe³⁺, respectively. (b) Fe 2p spectrum of V_{0.3}-CoFe-LDH was deconvoluted into two peaks at binding energies 708.1 eV and 723.5 eV assigned for 2p_{3/2} and 2p_{1/2} peaks, respectively. The Fe 2p_{3/2} was fitted into two peaks at binding energies 708.1 eV and 710.6 eV indicating the presence of Fe²⁺ and Fe³⁺, respectively. The peaks at 714.7 and 718.4 eV were the satellites of Fe²⁺ and Fe³⁺, respectively. The peaks at 2p_{3/2} and 2p_{1/2} showed the positive shift of 0.62 eV towards higher binding energy compared to the CoFe-LDH suggesting the strong electronic interaction among the elements.^[S8,S13-S15]

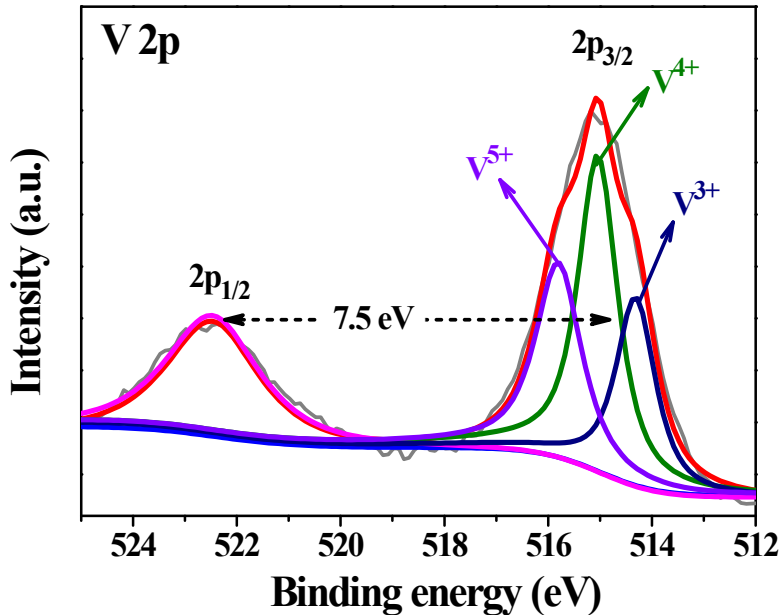


Figure S12. V 2p XP-spectrum of $\text{V}_{0.3}\text{-CoFe-LDH}$ was fitted into two peaks at binding energies 522.5 eV and 515.0 eV, assigned for $2\text{p}_{1/2}$ and $2\text{p}_{3/2}$ peaks, respectively. The peaks fitted at 514.3 eV, 515.0 eV, and 515.8 eV indicated to the presence of V^{3+} , V^{4+} , and V^{5+} , respectively, in $\text{V}_{0.3}\text{-CoFe-LDH}$.^[S1,S16-S17] The V 2p_{3/2} peaks displayed a significant negative shift of 0.9 eV and 1.9 eV compared to that of VO_2 and V_2O_5 , respectively indicating a strong electronic interaction of V with Co and Fe. Having empty e_g orbitals, V^{3+} ($3\text{d}^2/\text{t}_{2g}^2\text{e}_g^0$) ions can easily interact with H_2O molecules and protons to assist HER. In contrast, $\text{V}^{4+/5+}$ ions facilitate an optimum overlap of the Co 3d and Fe 3d orbitals and O 2p orbitals of oxygen intermediates below the Fermi level to increase the metal-oxygen covalency.^[S16-S17]

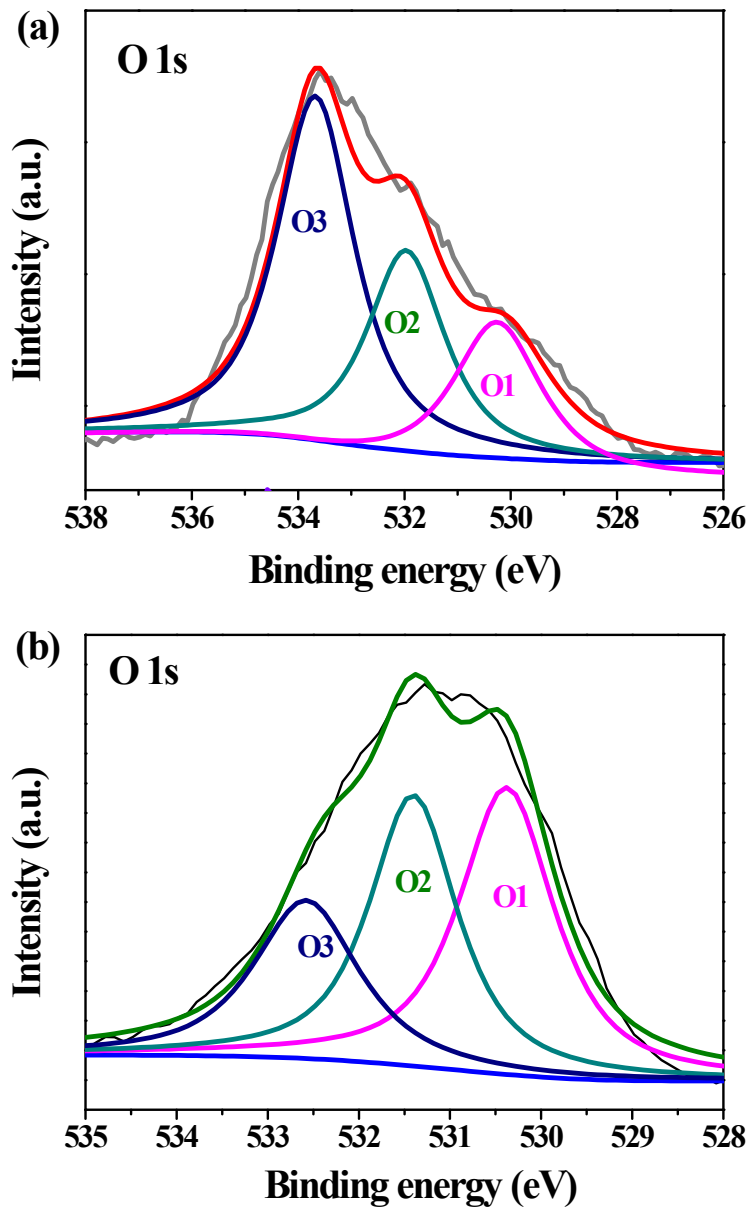


Figure S13. (a) O 1s XP-spectrum of CoFe-LDH showing the three peaks at 530.2 eV (O1), 532.0 eV (O2) and 533.6 eV (O3), corresponding to metal-oxygen bond, surface –OH groups and adsorbed water molecules. (b) O 1s XPS of $V_{0.3}$ -CoFe-LDH was deconvoluted into three peaks at 532.5 eV (O3), 531.4 eV (O2), and 530.4 eV (O1). The O3 and O2 peaks were assigned for the adsorbed water molecules and surface –OH groups whereas the O1 peak represented the metal-oxygen bond.^[S8-S12, S16-S17] A slight change of the peak positions (O1, O2 and O3) was recorded in $V_{0.3}$ -CoFe-LDH when compared with CoFe-LDH ascribed to the vanadium substitution.

Table S2. Comparison of the hydrogen evolution activity of V_{0.3}-CoFe-LDH with literature reported catalysts in alkaline solution.

Catalysts	Electrolyte	Current density (mA cm ⁻²)	Overpotential (mV)	References
<i>Our catalysts</i>				
CoFe-LDH	1 M aqueous KOH	10	270	This work
V _{0.1} -CoFe-LDH	1 M aqueous KOH	10	253	This work
V _{0.2} -CoFe-LDH	1 M aqueous KOH	10	215	This work
V_{0.3}-CoFe-LDH	1 M aqueous KOH	10	98	<i>This work</i>
V _{0.5} -CoFe-LDH	1 M aqueous KOH	10	250	This work
<i>Self-supported catalysts</i>				
Co-P/NC@CC	1 M aqueous KOH	10	171	S18
CoS ₂ @CC	1 M aqueous KOH	10	193	S19
CoSe ₂ @CFP	1 M aqueous KOH	10	113	S20
NiMoP ₂ @CC	1 M aqueous KOH	100	199	S21
CoP@CC	1 M aqueous KOH	10	95	S22
NiCoN@CC	1 M aqueous KOH	10	145	S23
NiFe ₂ O ₄ /NiFe-LDH@NF	1 M aqueous KOH	10	101	S24
CoNiP@NF	1 M aqueous KOH	10	155	S25
Co ₉ S ₈ -Ni _x S _y @NF	1 M aqueous KOH	10	163	S26
NiS@NF	1 M aqueous KOH	10	122	S27
<i>Layered double hydroxide catalysts</i>				
CoFe-LDH	1 M aqueous KOH	50	273	S28
NiFeV-LDH	1 M aqueous KOH	10	125	S16
NiFeMn-LDH	1 M aqueous KOH	10	110	S29
NiFe-LDH/NiSe	1 M aqueous KOH	10	276	S30
NiAl-LDH/MoS ₂	1 M aqueous KOH	10	220	S31
NiCoFe-LDH	1 M aqueous KOH	20	200	S32
CoMoV-LDH	1 M aqueous KOH	10	150	S33
<i>Vanadium-doped catalysts</i>				
V-WS ₂	1 M aqueous KOH	10	134	S34
V-CoP	1 M aqueous KOH	10	87	S35
V-CoP	1 M aqueous KOH	10	235	S36
V-Ni ₂ P	1 M aqueous KOH	10	85	S37
V-NiFe-LDH	1 M aqueous KOH	10	125	S16

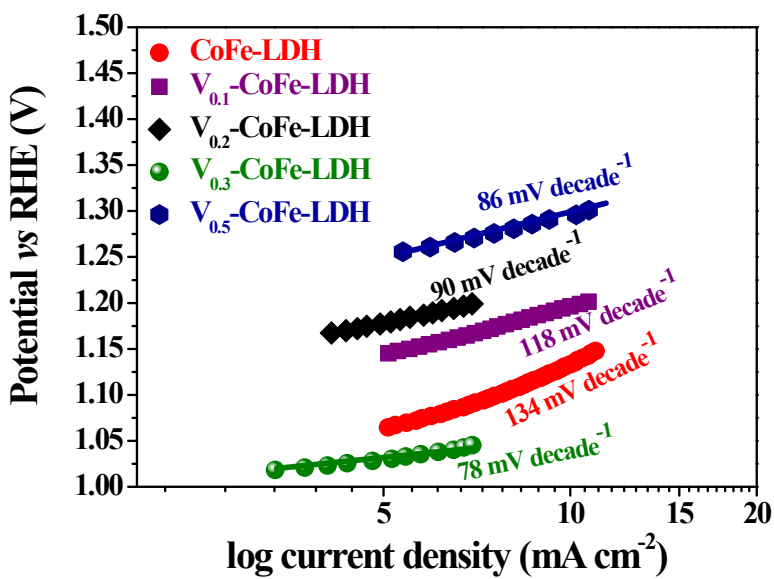


Figure S14. Tafel plots for the hydrogen evolution reaction of $V_{0.3}$ -CoFe-LDH compared with $V_{0.5}$ -CoFe-LDH, $V_{0.2}$ -CoFe-LDH, $V_{0.1}$ -CoFe-LDH, and CoFe-LDH showing the faster HER kinetics for $V_{0.3}$ -CoFe-LDH (Reaction conditions: scan rate 2 mV s⁻¹, aqueous 1.0 M KOH solution). The d-orbitals of low valent vanadium ($V^{3+} = 3d^2/t_{2g}^2e_g^0$) produce optimum interaction between the oxygen atom of H₂O and active sites favouring the adsorption/desorption behaviours of hydrogen atoms.^[S16-S17] As a result, vanadium substitution decreased the free energy of the Volmer step (*M-H-OH and *M-H) improving the HER kinetics in $V_{0.3}$ -CoFe-LDH. The lowest Tafel slope is observed for $V_{0.3}$ -CoFe-LDH (78 mV dec⁻¹) showing the faster HER kinetics compared to the synthesized catalysts.

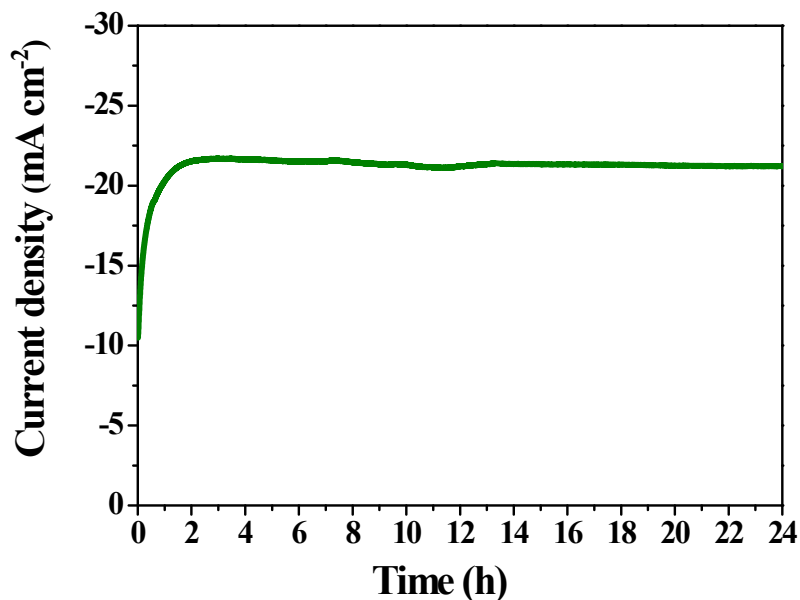


Figure S15. Chronoamperometric measurements for the hydrogen evolution reaction with $V_{0.3}$ -CoFe-LDH at 160 mV overpotential. The catalyst retained 99% current density up to 24 h showing the enhanced stability (Reaction condition: aqueous 1.0 M KOH solution).

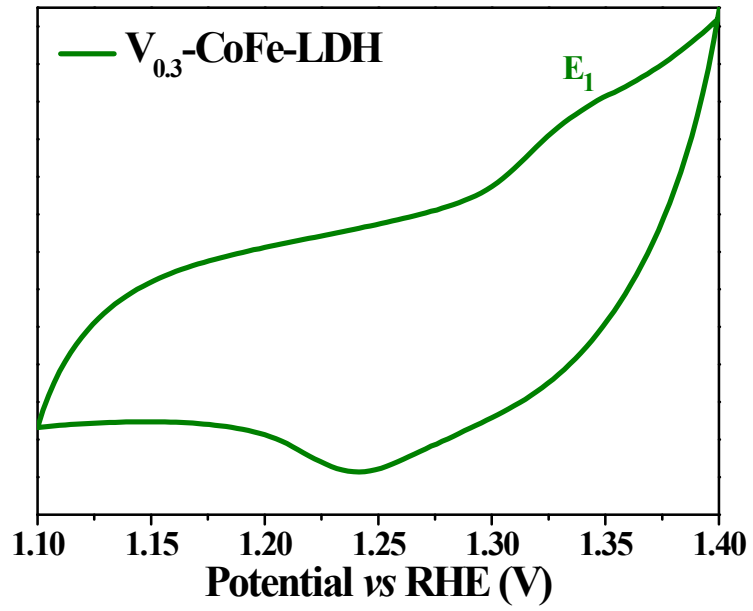


Figure S16. Short cyclic voltammetric profile of $\text{V}_{0.3}\text{-CoFe-LDH}$ during oxygen evolution reaction. The peak (E_1) was originated from the oxidation of Co^{2+} to Co^{3+} (Reaction conditions: scan rate 5 mV s⁻¹, aqueous 1.0 M KOH solution).^[S9-S12]

Table S3. Comparison of the oxygen evolution activity of V_{0.3}-CoFe-LDH with literature reported catalysts in alkaline electrolyte.

Catalysts	Electrolyte	Current density (mA cm ⁻²)	Overpotential (mV)	References
<i>Our catalysts</i>				
CoFe-LDH	1 M aqueous KOH	10	440	This work
V _{0.1} -CoFe-LDH	1 M aqueous KOH	10	270	This work
V_{0.2}-CoFe-LDH	1 M aqueous KOH	10	240	<i>This work</i>
V _{0.3} -CoFe-LDH	1 M aqueous KOH	10	240	This work
V _{0.5} -CoFe-LDH	1 M aqueous KOH	10	280	This work
<i>Self-supported catalysts</i>				
Co-P/NC@CC	1 M aqueous KOH	10	330	S18
CoMoO ₄ @CC	1 M aqueous KOH	10	290	S38
CoFe ₂ O ₄ @CC	1 M aqueous KOH	10	378	S39
NiMoP ₂ @CC	1 M aqueous KOH	100	330	S21
CoP@CC	1 M aqueous KOH	10	281	S22
(Ni,Co) _{0.85} Se@CC	1 M aqueous KOH	10	300	S40
<i>Layered double hydroxide catalysts</i>				
Co ₂ Fe-LDH	1 M aqueous KOH	10	420	S41
ZnCo-LDH	1 M aqueous KOH	10	340	S42
NiFe-LDH	1 M aqueous KOH	10	259	S43
CoMn-LDH	1 M aqueous KOH	10	350	S44
NiFe-LDH	1 M aqueous KOH	10	290	S45
CoCr-LDH	1 M aqueous KOH	20	400	S46
NiFe-LDH/CNT	1 M aqueous KOH	10	300	S47
CoFe-LDH	1 M aqueous KOH	10	280	S48
NiFeMo-LDH	1 M aqueous KOH	10	280	S49
CoMoV-LDH	1 M aqueous KOH	10	270	S33
<i>Vanadium-doped catalysts</i>				
V-CoS ₂	1 M aqueous KOH	10	290	S50
V-CoP	1 M aqueous KOH	10	340	S36
V-NiFe-LDH	1 M aqueous KOH	10	231	S26
V-NiMoN	1 M aqueous KOH	25	245	S51
V-NiP	1 M aqueous KOH	10	250	S52

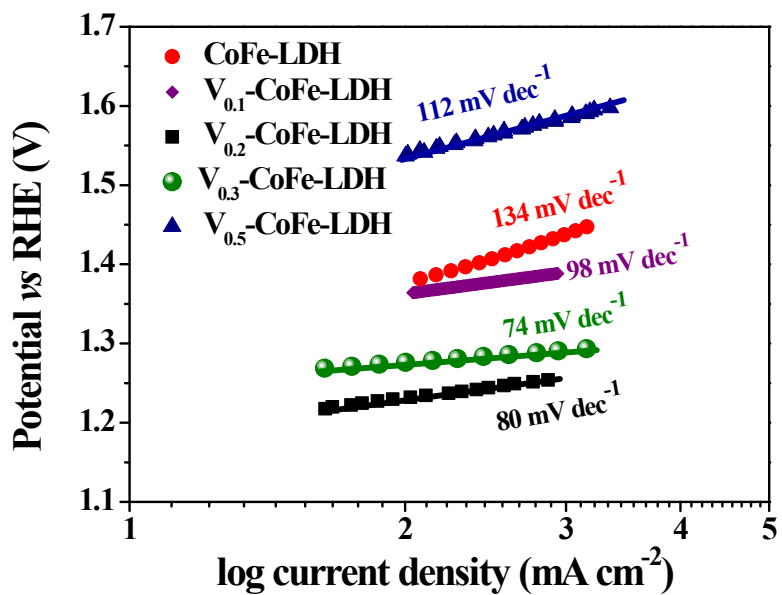


Figure S17. Tafel plots for the oxygen evolution reaction of $V_{0.3}$ -CoFe-LDH compared with $V_{0.5}$ -CoFe-LDH, $V_{0.2}$ -CoFe-LDH, $V_{0.1}$ -CoFe-LDH, and CoFe-LDH indicating the similar OER kinetics of $V_{0.3}$ -CoFe-LDH and $V_{0.2}$ -CoFe-LDH (Reaction conditions: scan rate 2 mV s^{-1} , aqueous 1.0 M KOH solution).

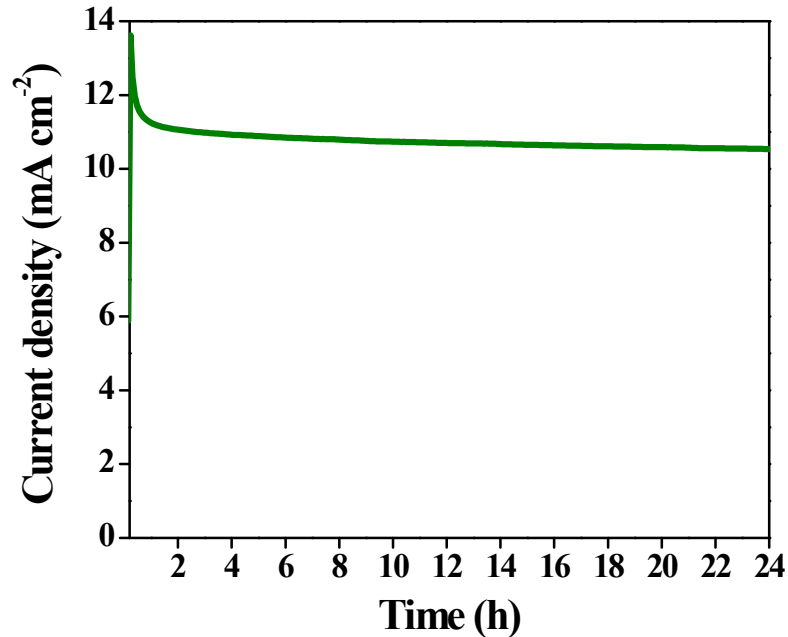


Figure S18. Chronoamperometric measurements for the oxygen evolution reaction with $V_{0.3}$ -CoFe-LDH at 1.48 V vs RHE. The catalyst retained 97% of initial current density up to 24 h showing the durability of the catalyst for continuous oxygen production (Reaction condition: aqueous 1.0 M KOH solution).

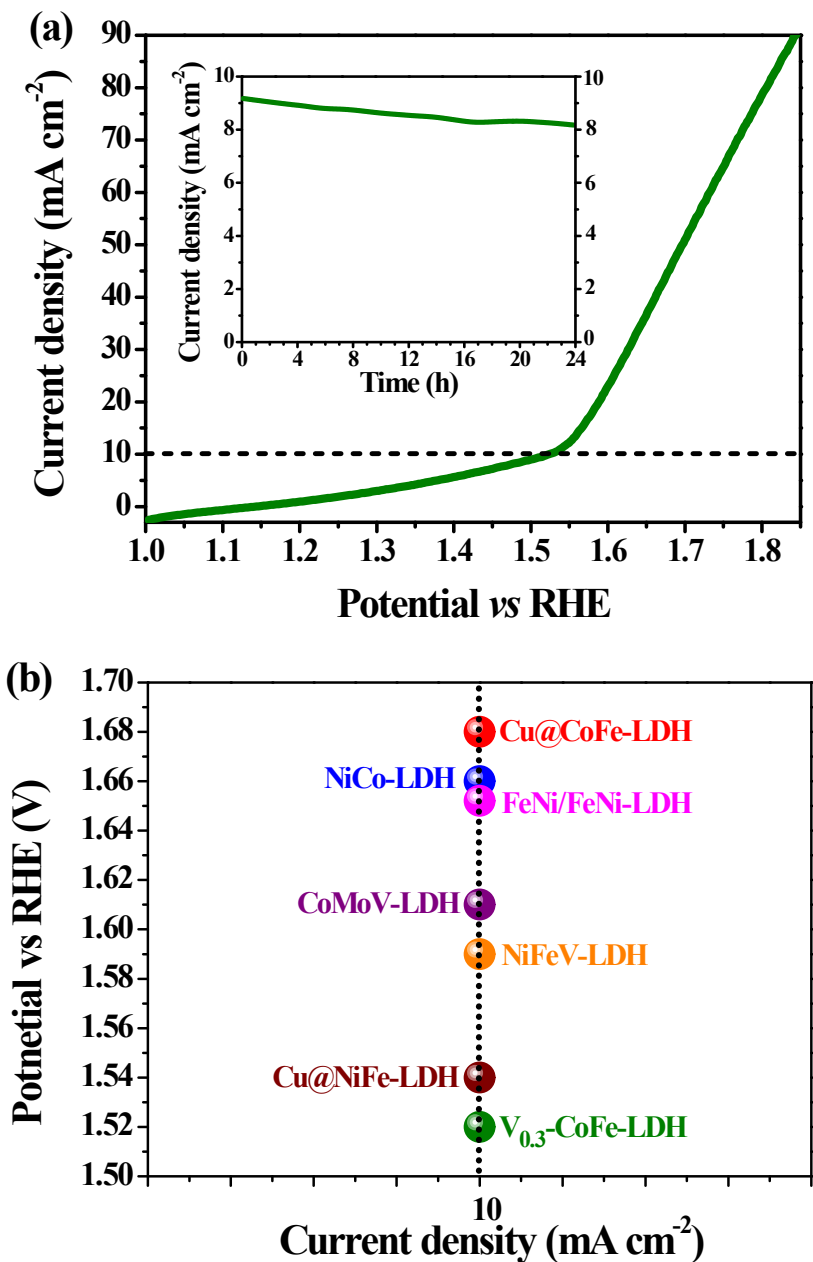


Figure S19. (a) Polarization curve of $\text{V}_{0.3}\text{-CoFe-LDH}$ for the overall water splitting (chronoamperometric stability test of $\text{V}_{0.3}\text{-CoFe-LDH}$ for 24 h at 1.55 V-inset) and (b) comparison of the overall water splitting activity of $\text{V}_{0.3}\text{-CoFe-LDH}$ with literature reported LDH catalysts.

Table S4. Comparison of the overall water splitting activity of V_{0.3}-CoFe-LDH with literature reported catalysts in alkaline electrolyte.

Catalysts	Electrolyte	Current density (mA cm ⁻²)	Cell Voltage (V)	References
<i>Our catalyst</i>				
V_{0.3}-CoFe-LDH	1 M aqueous KOH	10	1.52	This work
<i>Layered double hydroxide catalysts</i>				
CoMoV	1 M aqueous KOH	10	1.61	S33
NiCo-LDH	1 M aqueous KOH	10	1.66	S53
FeCo-LDH/GDY	1 M aqueous KOH	10	1.43	S54
NiFeV-LDH	1 M aqueous KOH	10	1.591	S26
NiFe LDH-NiSe	1 M aqueous KOH	10	1.53	S30
N-NiCo LDHs/NCF	1 M aqueous KOH	10	1.50	S55
Cu@CoFe-LDH	1 M aqueous KOH	10	1.68	S56
Rh-NiFe-LDH	1 M aqueous KOH	10	1.46	S57
Cu@NiFe-LDH	1 M aqueous KOH	10	1.54	S58
<i>Self-supported catalysts</i>				
Co-P/NC@CC	1 M aqueous KOH	10	1.70	S18
CoS ₂ @CC	1 M aqueous KOH	10	1.62	S19
Co ₃ S ₄ @CC	1 M aqueous KOH	10	1.55	S59
NiMoP ₂ @CC	1 M aqueous KOH	10	1.67	S21
CoP@CC	1 M aqueous KOH	10	1.61	S22
NiCoN@CC	1 M aqueous KOH	10	1.68	S23

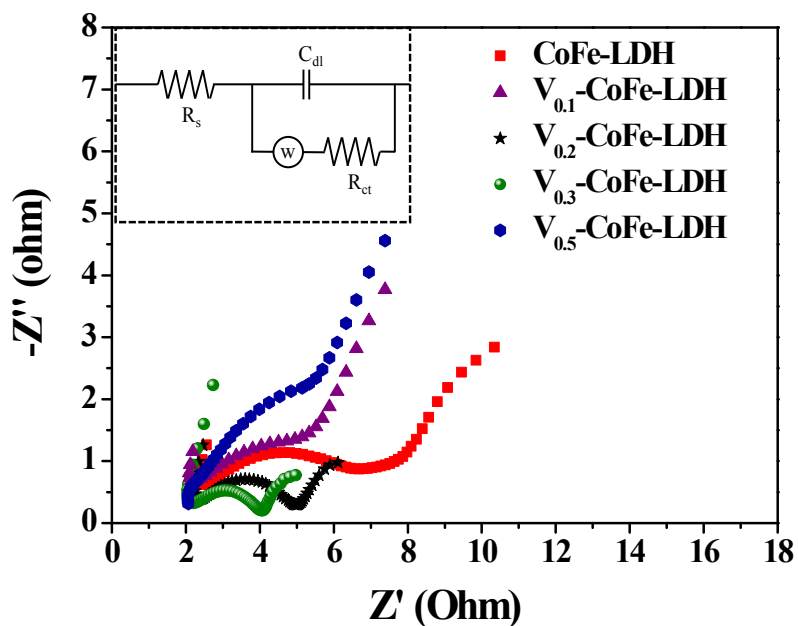


Figure S20. Nyquist plot showing the lowest charge transfer resistance for $V_{0.3}$ -CoFe-LDH compared with $V_{0.5}$ -CoFe-LDH, $V_{0.2}$ -CoFe-LDH, $V_{0.1}$ -CoFe-LDH, and CoFe-LDH. The lowest charge transfer resistance (R_{ct}) value was determined for $V_{0.3}$ -CoFe-LDH ($1.89\ \Omega$) compared to the $V_{0.5}$ -CoFe-LDH ($3.02\ \Omega$), $V_{0.2}$ -CoFe-LDH ($2.67\ \Omega$), $V_{0.1}$ -CoFe-LDH ($3.20\ \Omega$) and CoFe-LDH ($4.52\ \Omega$). It can be concluded here that the charge transfer resistance (R_{ct}) value was decreased after vanadium substitution when compared with the CoFe-LDH.

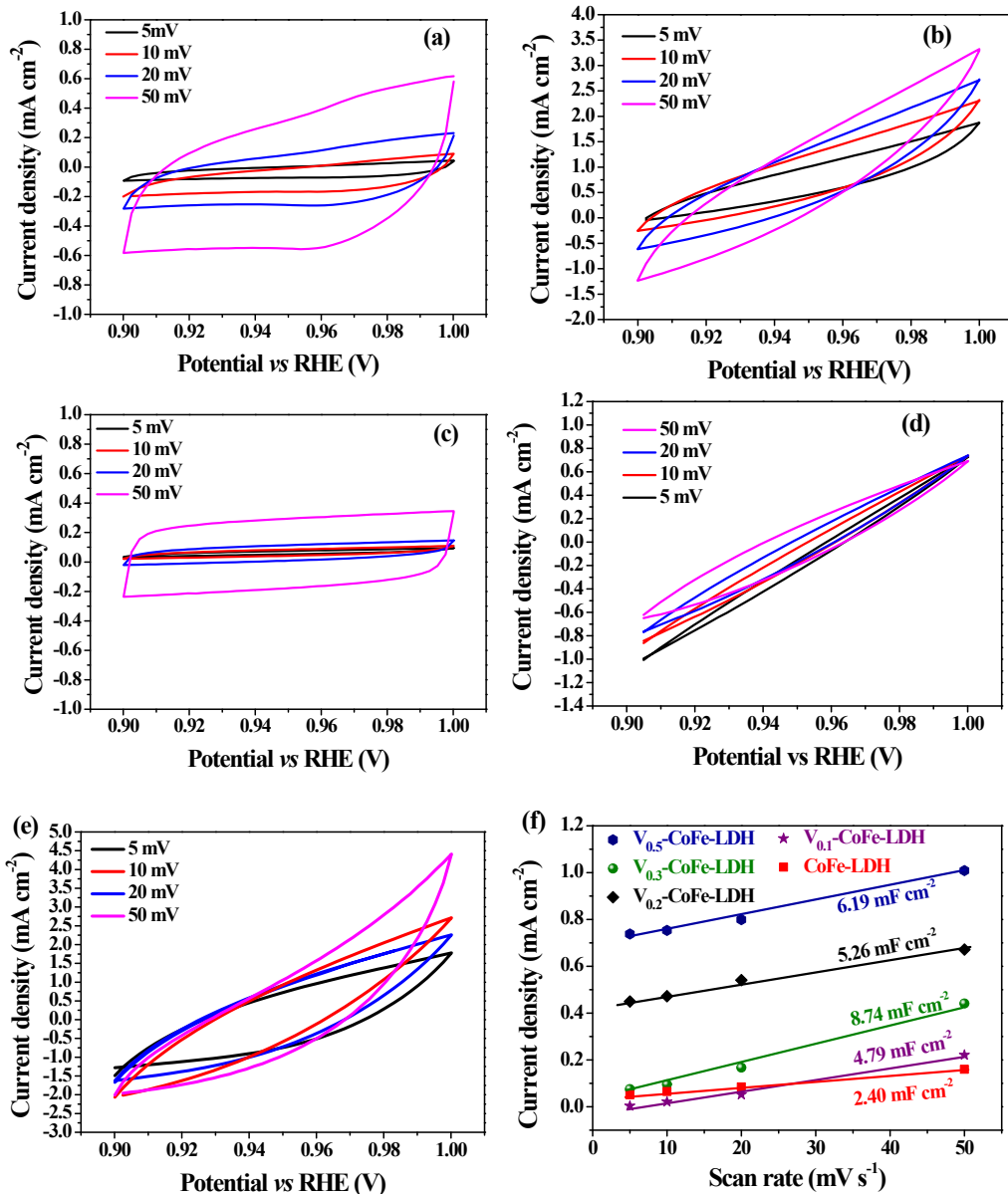


Figure S21. Electrochemical capacitance current of (a) $\text{V}_{0.3}\text{-CoFe-LDH}$, (b) $\text{V}_{0.2}\text{-CoFe-LDH}$, (c) $\text{V}_{0.1}\text{-CoFe-LDH}$, (d) CoFe-LDH, and (e) $\text{V}_{0.5}\text{-CoFe-LDH}$ in the non-Faradaic potential range of 0.90 V to 1.00 V vs RHE and (f) determination of double-layer capacitance (C_{dl}) by plotting (difference in current density)/2 against scan rate. The specific capacitance of 1 cm² flat surface area is in the range of 20-60 $\mu\text{F cm}^{-2}$, which can be averaged to 40 $\mu\text{F cm}^{-2}$. The C_{dl} value was converted to the electrochemical surface area (ECSA) using the equation: $\text{ECSA} = C_{\text{dl}} \text{ of catalyst in mF} / 0.04 \text{ mF cm}^{-2}$ [S60-S61]

$$\text{ECSA of } \text{V}_{0.5}\text{-CoFe-LDH} = 6.19 / 0.04 = 154.75 \text{ cm}^2 / 2.3 \text{ mg} = 67.28 \pm 2.01 \text{ cm}^2/\text{mg}$$

$$\text{ECSA of } \text{V}_{0.3}\text{-CoFe-LDH} = 8.74 / 0.04 = 218.50 \text{ cm}^2 / 2.5 \text{ mg} = 87.40 \pm 2.62 \text{ cm}^2/\text{mg}$$

$$\text{ECSA of } \text{V}_{0.2}\text{-CoFe-LDH} = 5.26 / 0.04 = 131.50 \text{ cm}^2 / 2.4 \text{ mg} = 54.79 \pm 1.36 \text{ cm}^2/\text{mg}$$

$$\text{ECSA of } \text{V}_{0.1}\text{-CoFe-LDH} = 4.29 / 0.04 = 107.25 \text{ cm}^2 / 2.3 \text{ mg} = 46.63 \pm 1.86 \text{ cm}^2/\text{mg}$$

$$\text{ECSA of CoFe-LDH} = 2.40 / 0.04 = 60.00 \text{ cm}^2 / 2.4 \text{ mg} = 25.00 \pm 1.25 \text{ cm}^2/\text{mg}$$

The increment in ECSA was observed when compared with the CoFe-LDH after the vanadium substitution.

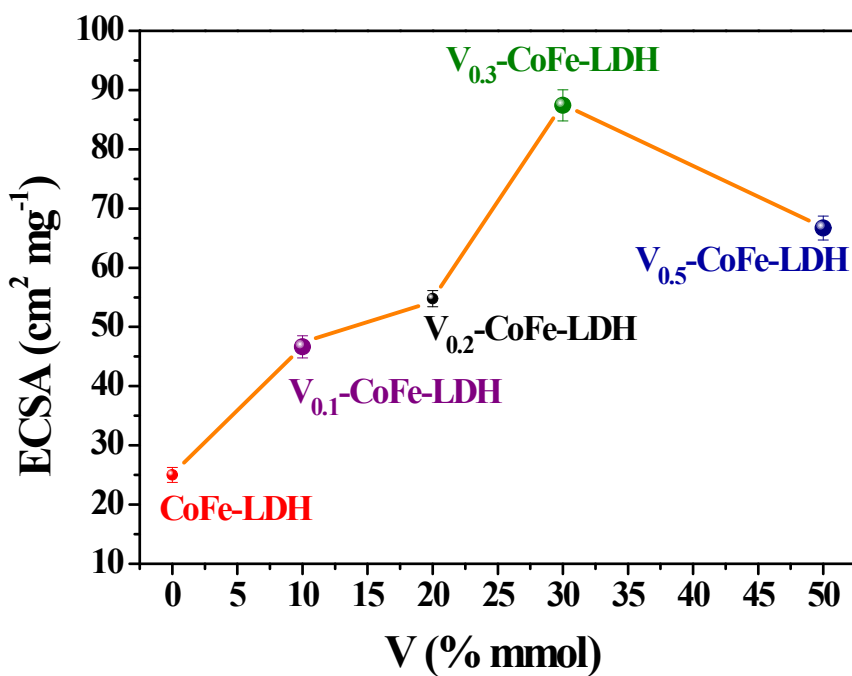


Figure S22. Plot of ECSA vs vanadium content in V_{0.5}-CoFe-LDH, V_{0.3}-CoFe-LDH, V_{0.2}-CoFe-LDH, V_{0.1}-CoFe-LDH, and CoFe-LDH. The plot shows that the ECSA is increased up to V_{0.3}-CoFe-LDH with increase in the vanadium substitution after that no increment in ECSA is observed. This indicates that there is a limit of vanadium substitution to increase the ECSA.

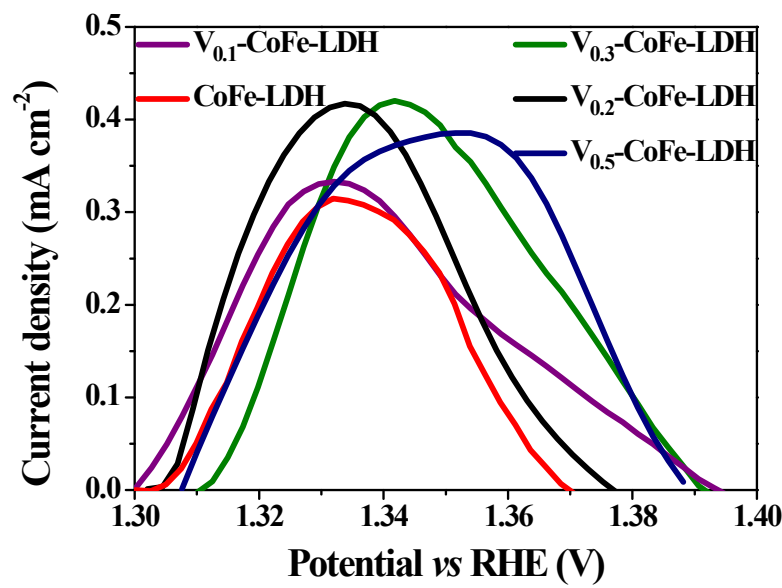


Figure S23. Potential vs current density plots showing the oxidation peak used for the area integration to calculate the surface active sites of V_{0.5}-CoFe-LDH, V_{0.3}-CoFe-LDH, V_{0.2}-CoFe-LDH, V_{0.1}-CoFe-LDH, and CoFe-LDH catalyst.^[S62-S63]

Equation S1: Determination of surface active sites using area integration of oxidation peak.^[S62-S63]

For V_{0.5}-CoFe-LDH

Calculated area associated with the oxidation peak = 0.01756×10^{-3} V A

Hence the associated charge is = 0.01756×10^{-3} V A / 0.005 V s^{-1}

$$= 3.512 \times 10^{-3} \text{ A s}$$

$$= 3.512 \times 10^{-3} \text{ C}$$

Now, the number of electron transferred is = $3.512 \times 10^{-3} \text{ C} / 1.602 \times 10^{-19} \text{ C}$

$$= 2.19 \times 10^{16}$$

Since the oxidation of Co²⁺ to Co³⁺ is a single electron transfer reaction, the number of electrons calculated above is the same as the number of surface active sites.

Hence,

The surface-active site that participated in OER is = **(2.19±0.03)×10¹⁶**

For V_{0.3}-CoFe-LDH

Calculated area associated with the oxidation peak = 0.01802×10^{-3} V A

Hence the associated charge is = 0.01802×10^{-3} V A / 0.005 V s^{-1}

$$= 3.604 \times 10^{-3} \text{ As}$$

$$= 3.604 \times 10^{-3} \text{ C}$$

Now, the number of electron transferred is = $3.604 \times 10^{-3} \text{ C} / 1.602 \times 10^{-19} \text{ C}$

$$= 2.24 \times 10^{16}$$

The surface-active site that participated in OER is = **(2.24±0.02)×10¹⁶**

For V_{0.2}-CoFe-LDH

Calculated area associated with the oxidation peak = 0.01638×10^{-3} V A

Hence the associated charge is = 0.01638×10^{-3} V A / 0.005 V s^{-1}

$$= 3.276 \times 10^{-3} \text{ As}$$

$$= 3.276 \times 10^{-3} \text{ C}$$

Now, the number of electron transferred is = $3.276 \times 10^{-3} \text{ C} / 1.602 \times 10^{-19} \text{ C}$

$$= 2.0 \times 10^{16}$$

The surface active site that participated in OER is = **(2.04±0.04)×10¹⁶**

For V_{0.1}-CoFe-LDH

Calculated area associated with the oxidation peak = 0.01547×10^{-3} V A

Hence the associated charge is = 0.01547×10^{-3} V A / 0.005 V s^{-1}

$$= 3.042 \times 10^{-3} \text{ As}$$

$$= 3.042 \times 10^{-3} \text{ C}$$

Now, the number of electron transferred is = $3.042 \times 10^{-3} \text{ C} / 1.602 \times 10^{-19} \text{ C}$

$$= 1.90 \times 10^{16}$$

The surface active site that participated in OER is = **(1.90±0.03)×10¹⁶**

For CoFe-LDH

Calculated area associated with the oxidation peak = $0.01499 \times 10^{-3} \text{ V A}$

Hence the associated charge is = $0.01499 \times 10^{-3} \text{ V A}/0.005 \text{ V s}^{-1}$

$$= 2.998 \times 10^{-3} \text{ As}$$

$$= 2.998 \times 10^{-3} \text{ C}$$

Now, the number of electron transferred is = $2.998 \text{ C} \times 10^{-3} / 1.602 \times 10^{-19} \text{ C}$

$$= 1.87 \times 10^{16}$$

The surface active site that participated in OER is = $(1.87 \pm 0.03) \times 10^{16}$

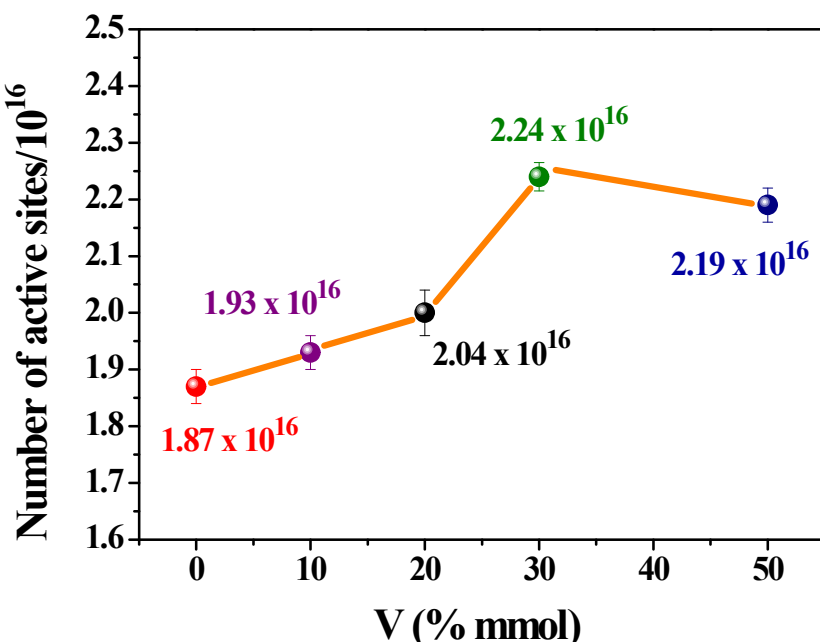


Figure S24. Plot for the number of active sites vs vanadium content in $\text{V}_{0.5}\text{-CoFe-LDH}$, $\text{V}_{0.3}\text{-CoFe-LDH}$, $\text{V}_{0.2}\text{-CoFe-LDH}$, $\text{V}_{0.1}\text{-CoFe-LDH}$, and CoFe-LDH. The number of active sites is increased continuously with the vanadium substitution up to $\text{V}_{0.3}\text{-CoFe-LDH}$ and further decreases in $\text{V}_{0.5}\text{-CoFe-LDH}$. The plot suggests that there is a limit of increasing the number of active sites by vanadium substitution.

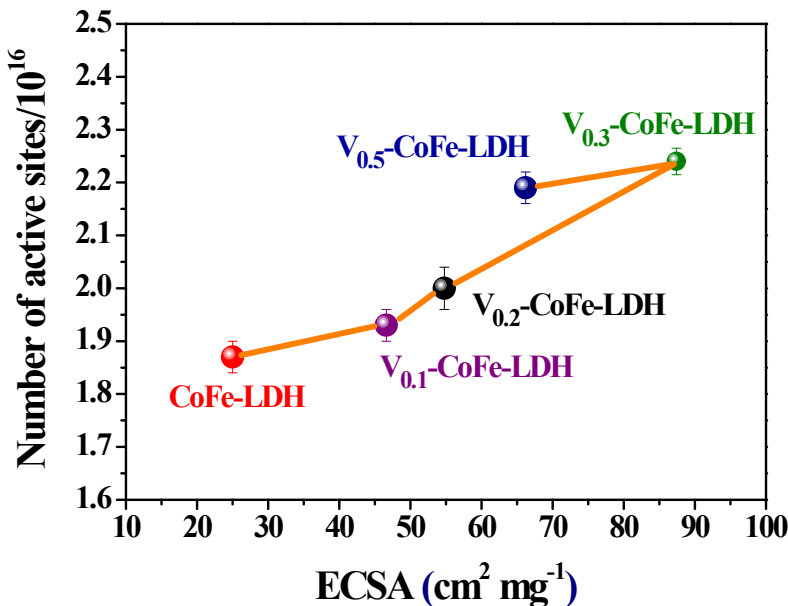


Figure S25. Plot for the number of active sites vs ECSA in $\text{V}_{0.5}\text{-CoFe-LDH}$, $\text{V}_{0.3}\text{-CoFe-LDH}$, $\text{V}_{0.2}\text{-CoFe-LDH}$, $\text{V}_{0.1}\text{-CoFe-LDH}$, and CoFe-LDH. The plot indicates that ECSA and number of active sites is increased up to $\text{V}_{0.3}\text{-CoFe-LDH}$ with increasing vanadium substitution after that number of actives sites and ECSA is decreased in $\text{V}_{0.5}\text{-CoFe-LDH}$ with increasing vanadium substitution.

Equation S2. Calculation of Turn over frequency (TOF) of different catalysts.^[S62-S63]

$$\text{TOF} = (j \times N_A) / (4 \times F \times n)$$

Where,

j = current density at $\eta = 240 \text{ mV}$

N_A = Avogadro number

F = Faraday constant

n = number of active Co-sites

For $\text{V}_{0.5}\text{-CoFe-LDH}$

$$\text{TOF} = [(6.97 \times 10^{-3}) (6.023 \times 10^{23})] / [(96485) (4) (2.19 \times 10^{16})]$$

$$\text{TOF} = 0.490 \pm 0.026 \text{ s}^{-1}$$

For $\text{V}_{0.3}\text{-CoFe-LDH}$

$$\text{TOF} = [(10.00 \times 10^{-3}) (6.023 \times 10^{23})] / [(96485) (4) (2.24 \times 10^{16})]$$

$$\text{TOF} = 0.691 \pm 0.027 \text{ s}^{-1}$$

For V_{0.2}-CoFe-LDH

$$\text{TOF} = [(10.00 \times 10^{-3}) (6.023 \times 10^{23})] / [(96485) (4) (2.04 \times 10^{16})]$$

$$\text{TOF} = 0.761 \pm 0.028 \text{ s}^{-1}$$

For V_{0.1}-CoFe-LDH

$$\text{TOF} = [(6.34 \times 10^{-3}) (6.023 \times 10^{23})] / [(96485) (4) (1.90 \times 10^{16})]$$

$$\text{TOF} = 0.522 \pm 0.020 \text{ s}^{-1}$$

For CoFe-LDH

$$\text{TOF} = [(0.95 \times 10^{-3}) (6.023 \times 10^{23})] / [(96485) (4) (1.87 \times 10^{16})]$$

$$\text{TOF} = 0.073 \pm 0.005 \text{ s}^{-1}$$

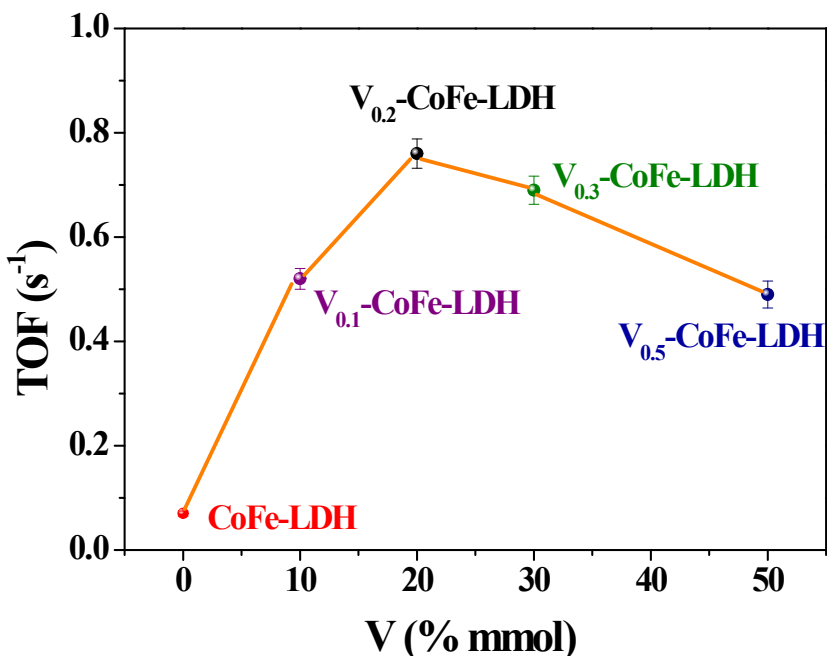


Figure S26. Plot for the turn over frequency (TOF) *vs* vanadium content in V_{0.5}-CoFe-LDH (0.490±0.026 s^{-1}), V_{0.3}-CoFe-LDH (0.691±0.027 s^{-1}), V_{0.2}-CoFe-LDH (0.761±0.028 s^{-1}), V_{0.1}-CoFe-LDH (0.522±0.020 s^{-1}), and CoFe-LDH (0.073±0.005 s^{-1}). The TOF is increased up to V_{0.3}-CoFe-LDH with increase in vanadium substitution and further decreases in V_{0.5}-CoFe-LDH.

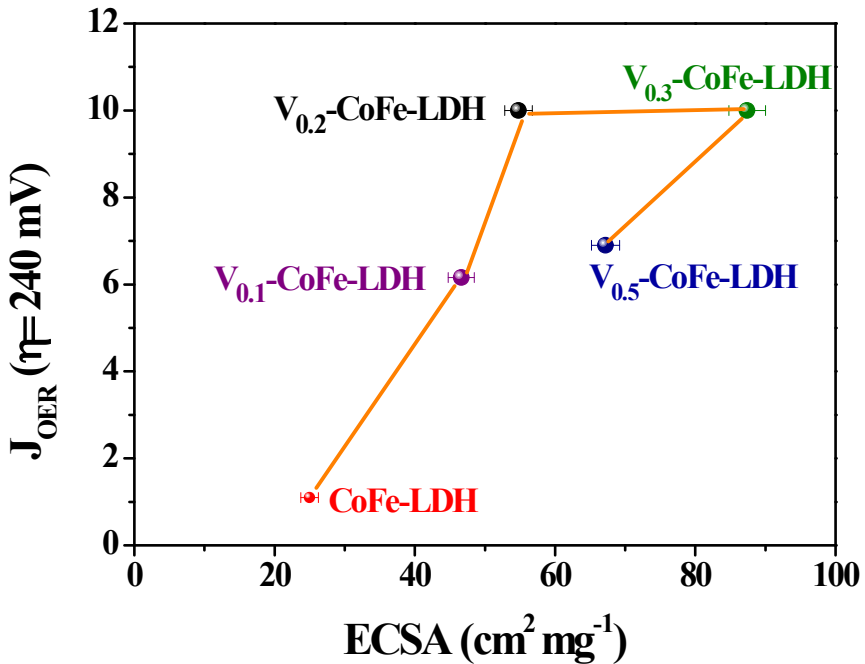


Figure S27. The OER current density of different catalysts attained at 240 overpotential ($J_{\eta=240}$) plotted against ECSA.

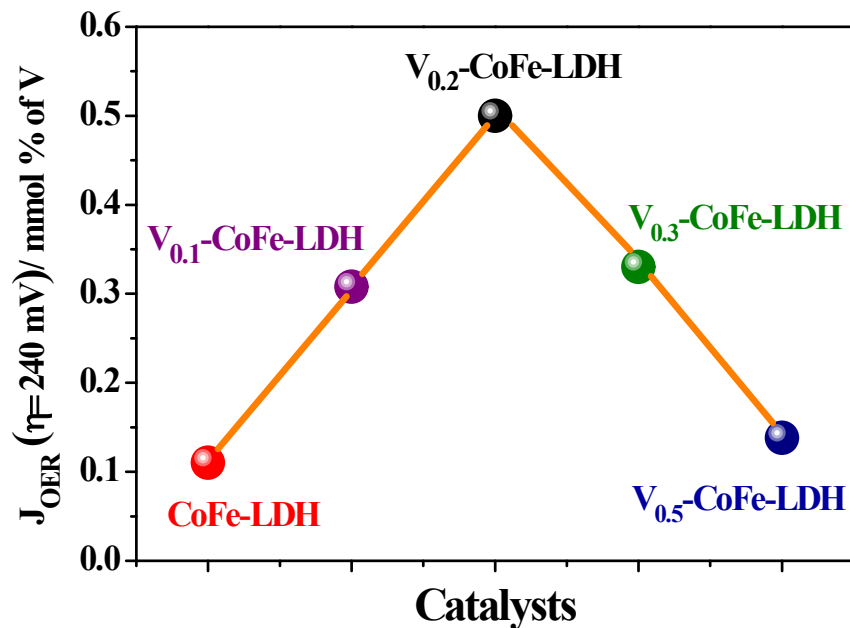


Figure S28. Plot for the OER current density ($J_{\eta=240}$) of different catalysts normalized with vanadium content.

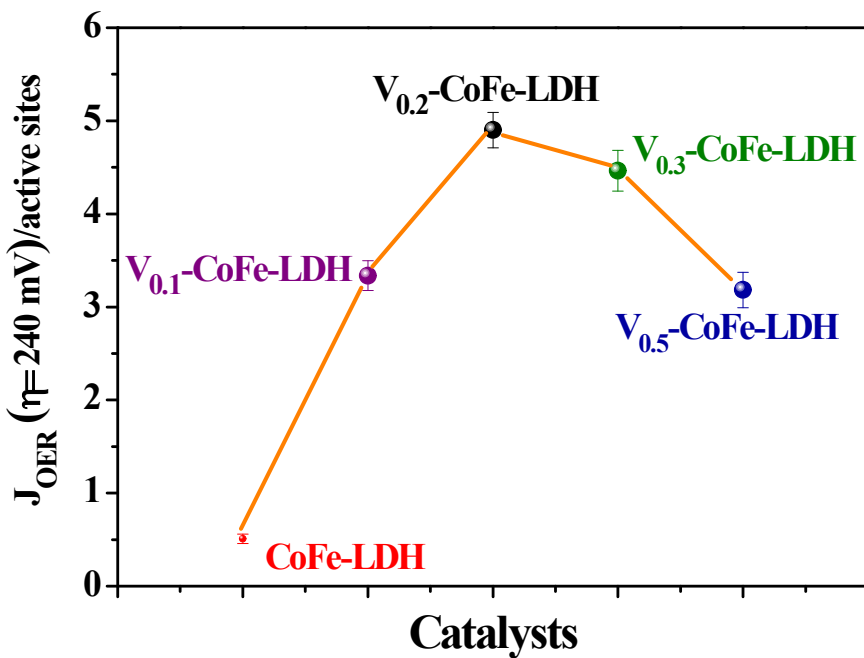


Figure S29. Plot for the OER current density ($J_{\eta=240}$) normalized with number of active sites.

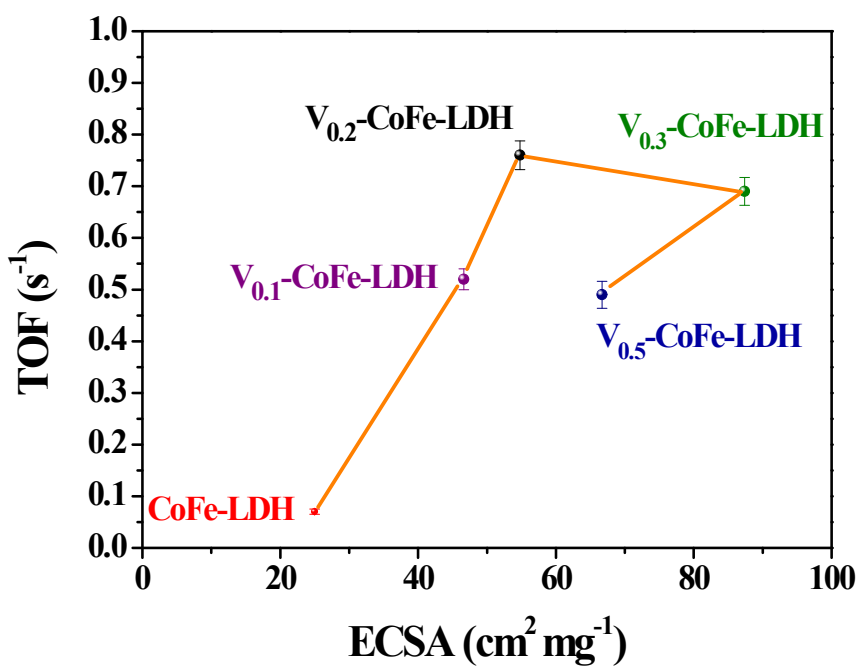


Figure S30. Plot for the TOF vs ECSA for the different synthesized catalysts. The plot indicates the highest intrinsic activity of $V_{0.2}\text{-CoFe-LDH}$ among the synthesized catalysts.

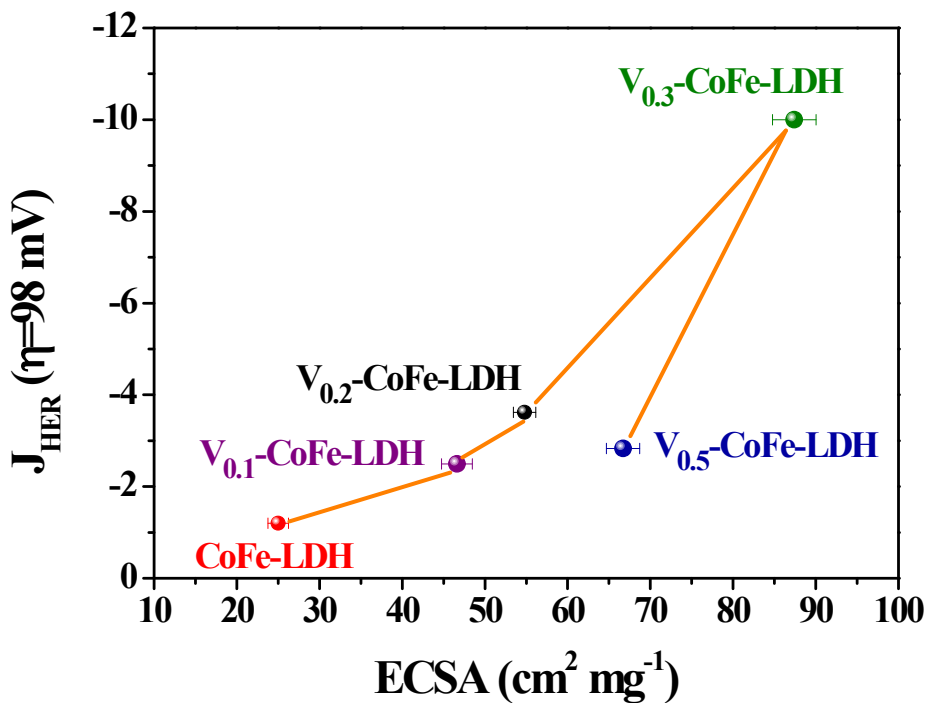


Figure S31. HER current density of different catalysts at 98 mV overpotential ($J_{\eta=98 \text{ mV}}$) plotted against ECSA, indicating the increased current density with increase in ECSA.

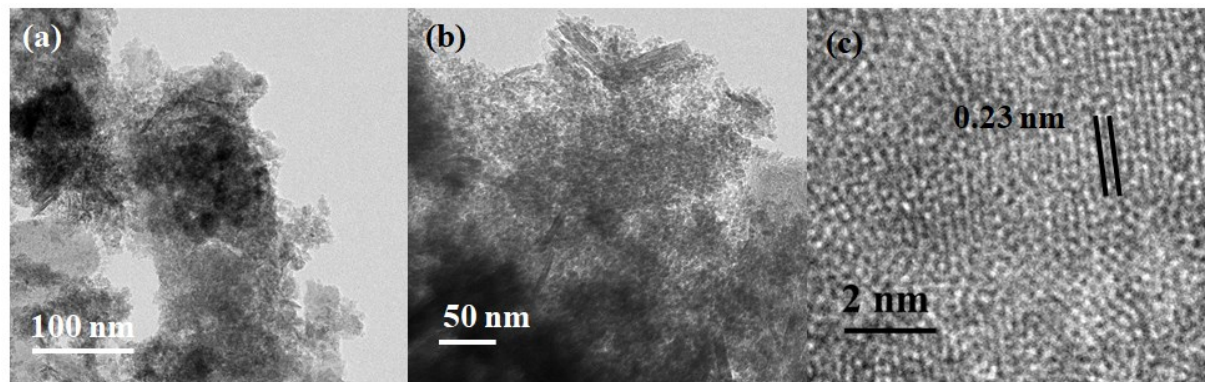


Figure S32. (a-b) TEM images of $V_{0.3}\text{-CoFe-LDH}$ after OER-CA showing slight agglomeration of the nanosheets; (c) HRTEM image detects the inter-planar spacing of 0.23 nm assigned for (111) plane of $\beta\text{-Co(O)OH}$ formed during OER (JCPDS No. 26-480).

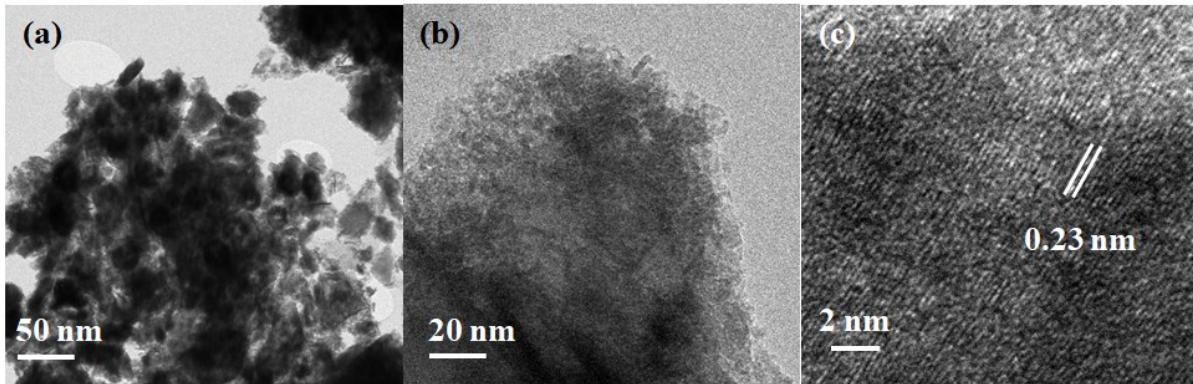


Figure S33. (a-b) TEM images of $V_{0.3}$ -CoFe-LDH after HER-CA showing the agglomerated nanosheets; (c) HRTEM image detects the inter-planar spacing of 0.23 nm assigned for (002) plane of α -Co(OH)₂ (JCPDS No. 30-443).

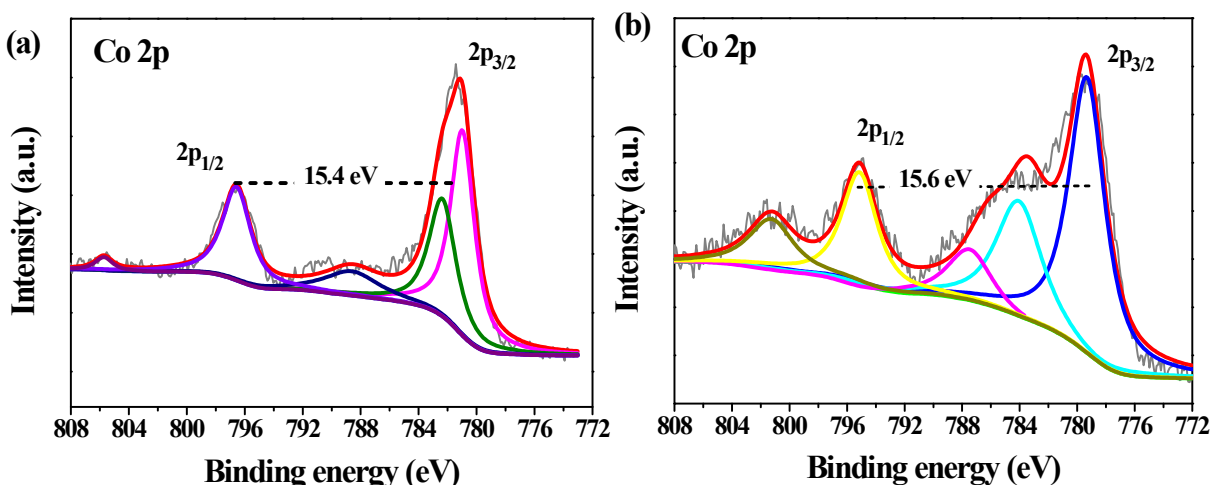


Figure S34. (a) Co 2p XP-spectrum of $V_{0.3}$ -CoFe-LDH after OER-CA deconvoluted into two peaks at 796.5 eV and 781.1 eV binding energies assigned for $2p_{1/2}$ and $2p_{3/2}$, respectively. The peaks at 780.9 eV and 782.4 eV were assigned for Co^{3+} and Co^{2+} , respectively. After OER-CA, spin-orbit coupling spacing was observed to be decreased to 15.4 eV from 15.7 eV in the fresh catalyst. This result indicates that Co^{2+} is partially oxidized to Co^{3+} during the anodic water oxidation. Therefore, the Co^{3+}/Co^{2+} peak ratio was found to be higher (1.73) after OER-CA than that of the fresh catalyst (1.52). (b) Co 2p XP-spectrum of $V_{0.3}$ -CoFe-LDH after HER-CA deconvoluted into two peaks at the binding energies 779.4 eV and 795.0 eV corresponding to $2p_{3/2}$ and $2p_{1/2}$, respectively. The peaks at 779.4 eV and 784.2 eV were assigned for Co^{3+} and Co^{2+} , respectively.^[S8-S12] After HER-CA, the Co^{3+}/Co^{2+} peak ratio (1.37) was calculated to be lower than that of the OER catalyst. The spin orbit coupling spacing (15.6 eV) also showed a relatively higher amount of Co^{2+} after HER than that of the OER catalyst.

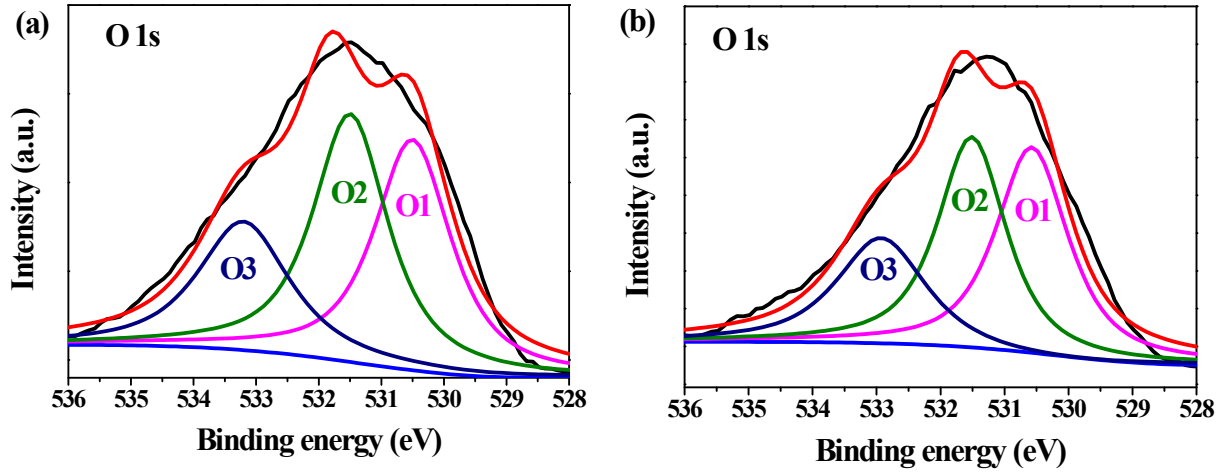


Figure S35. (a) O 1s XP-spectrum of $\text{V}_{0.3}\text{-CoFe-LDH}$ after OER-CA showed three peaks at 533.2 eV (O3), 531.4 eV (O2) and 530.5 (O1) eV binding energies, which were attributed to the adsorbed water molecules, surface –OH groups and metal–oxygen bond, respectively. The O2/O1 ratio after OER-CA was determined to be 1.11 higher than that of the fresh $\text{V}_{0.3}\text{-CoFe-LDH}$ (0.98) indicating hydroxylation of the catalyst during water oxidation. (b) O 1s XP-spectrum of $\text{V}_{0.3}\text{-CoFe-LDH}$ after HER-CA showing the peaks at 530.5 eV (O1), 531.5 eV (O2) and 532.9 eV (O3), assigned for metal–oxygen bond, surface –OH group and adsorbed water molecules, respectively. The O1 peak showed an increment in the peak area after HER-CA and OER-CA compared to the fresh catalyst suggested the formation of more metal–oxygen bond due to oxidation of Co(II) to Co(III) to form Co(O)OH species.^[S8-S12,S16-S17]

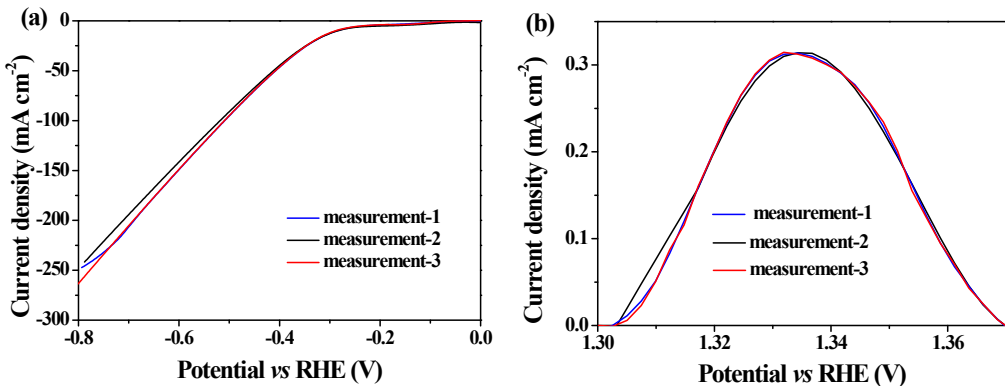


Figure S36. (a) HER-LSV profile of CoFe-LDH showing the measurements for the three set of experiments and (b) Potential vs current density plots for CoFe-LDH showing the three set of experiments used for the area integration to calculate the surface active sites. For all the electrochemical data, the average of three concomitant set of experiments has been presented. If error was more than 10%, we have discarded the point of the data set.

References

- [S1] Y. Hu, Z. Wang, W. Liu, L. Xu, M. Guan, Y. Huang, Y. Zhao, J. Bao, H. -ming. Li, *ACS Sustainable Chem. Eng.* **2019**, *7*, 16828-16834.
- [S2] J. Jiang, F. Sun, S. Zhou, W. Hu, H. Zhang, J. Dong, Z. Jiang, J. Zhao, J. Li, W. Yan, M. Wang, *Nat. Commun.* **2018**, *9*, 2885.
- [S3] D. Wang, Q. Li, C. Han, Q. Lu, Z. Xing, X. Yang, *Nat. Commun.* **2019**, *10*, 3899.
- [S4] M. Tathavadekara, M. Biswala, S. Agarkara, L. Giribabuc, S. Ogalea, *Electrochimica Acta*. **2014**, *123*, 248-253.
- [S5] N. K. Gupta, M. Saifuddin, S. Kim, K. S. Kim, *J. Mol. Liq.* **2020**, *297*, 111935.
- [S6] T. -J. Wang, X. Liu, Y. Li, F. Li, Z. Deng, Y. Chen, *Nano Res.* **2020**, *13*, 79-85.
- [S7] S. Liu, J. Zhu, M. Sun, Z. Ma, K. Hu, T. Nakajima, X. Liu, P. Schmuki, L. Wang, *J. Mater. Chem. A* **2020**, *8*, 2490-2497.
- [S8] M. Fantauzzi, F. Secci, M. S. Angotzi, C. Passiu, C. Cannas, A. Rossi, *RSC Adv.* **2019**, *9*, 19171-19179.
- [S9] A. Indra, P. W. Menezes, I. Zaharieva, H. Dau, M. Driess, *J. Mater. Chem. A* **2020**, *8*, 2637-2643.
- [S10] A. Indra, P. W. Menezes, C. Das, C. Göbel, M. Tallarida, D. Schmeißer, M. Driess, *J. Mater. Chem. A* **2017**, *5*, 5171-5177.
- [S11] A. Indra, P. W. Menezes, C. Das, D. Schmeißer, M. Driess, *Chem. Commun.* **2017**, *53*, 8641-8644.
- [S12] P. W. Menezes, A. Indra, I. Zaharieva, C. Walter, S. Loos, S. Hoffmann, R. Schlögl, H. Dau, M. Driess, *Energy Environ. Sci.* **2019**, *12*, 988-999.
- [S13] T. Yamashita, P. Hayes, *Appl. Surf. Sci.* **2008**, *254*, 2441-2449.
- [S14] M. C. Biesinger, B. P. Payne, A. P. Grosvenor, L. W. M. Lau, A. R. Gerson, R. St. C. Smart, *Appl. Surf. Sci.* **2011**, *257*, 2717-2730.
- [S15] A. P. Grosvenor, B. A. Kobe, M. C. Biesinger, N. S. McIntyre, *Surf. Interface Anal.* **2004**, *36*, 1564-1574
- [S16] (a) K. N. Dinh, P. Zheng, Z. Dai, Y. Zhang, R. Dangol, Y. Zheng, B. Li, Y. Zong, Q. Yan, *Small* **2018**, *14*, 1703257; (b) D. He, L. Cao, J. Huang, K. Kajiyoshi, J. Wu, C. Wang, Q. Liu, D. Yang, L. Feng, *J. Energy Chem.* **2020**, *47*, 263-271.
- [S17] (a) P. Li, X. Duan, Y. Kuang, Y. Li, G. Zhang, W. Liu, X. Sun, *Adv. Energy Mater.* **2018**, *8*, 1703341; (b) Y. Yang, Y. Ou, Y. Yang, X. Wei, D. Gao, L. Yang, Y. Xiong, H. Dong, P. Xiao, Y. Zhang, *Nanoscale* **2019**, *11*, 23296-23303.
- [S18] X. Liu, J. Dong, B. You, Y. Sun, *RSC Adv.* **2016**, *6*, 73336-73342.
- [S19] C. Guan, X. Liu, A. M. Elshahawy, H. Zhang, H. Wu, S. J. Pennycook, J. Wang, *Nanoscale Horiz.* **2017**, *2*, 342-348.
- [S20] C. Sun, Q. Dong, J. Yang, Z. Dai, J. Lin, P. Chen, W. Huang, X. Dong, *Nano. Res.* **2016**, *8*, 2234-2243.
- [S21] X. -D. Wang, H. -Y. Chen, Y. -F. Xu, J. -F. Liao, B. -X. Chen, H. -S. Rao, D. -B. Kuang, C. -Y. Su, *J. Mater. Chem. A* **2017**, *5*, 7191-7199.
- [S22] P. Wang, F. Song, R. Amal, Y. H. Ng, X. Hu, *ChemSusChem* **2016**, *9*, 472-477.
- [S23] L. Han, K. Feng, Z. Chen, *Energy Technol.* **2017**, *5*, 1908-1911.

- [S24] Z. Wu, Z. Zou, J. Huang, F. Gao, *ACS Appl. Mater. Interfaces* **2018**, *10*, 26283-26292.
- [S25] A. Han, H. Chen, H. Zhang, Z. Sun, P. Du, *J. Mater. Chem. A* **2016**, *4*, 10195-10202.
- [S26] D. Ansovini, C. J. J. Lee, C. S. Chua, L. T. Ong, H. R. Tan, W. R. Webb, R. Raja, Y. -F. Lim, *J. Mater. Chem. A* **2016**, *4*, 9744-9749.
- [S27] J. -T. Ren, Z. -Y. Yuan, *ACS Sustainable Chem. Eng.* **2017**, *5*, 7203-7210.
- [S28] G.; Rajeshkhanna, T. I. Singh, N. H. Kim, J. H. Lee, *ACS Appl. Mater. Interfaces* **2018**, *10*, 42453-42468.
- [S29] L. Yan, Y. Ren, X. Zhang, Y. Sun, J. Ning, Y. Zhong, B. Teng, Y. Hu, *Nanoscale* **2019**, *11*, 20797-20808.
- [S30] S. Dutta, A. Indra, Y. Feng, T. Song, U. Paik, *ACS Appl. Mater. Interfaces* **2017**, *9*, 33766-33774.
- [S31] M. S. Islam, M. Kim, X. Jin, S. M. Oh, N. -S. Lee, H. Kim, S. -J. Hwang, *ACS Energy Lett.* **2018**, *3*, 952-960.
- [S32] A. -L. Wang, H. Xu, G. -R. Li, *ACS Energy Lett.* **2016**, *1*, 445-453.
- [S33] J. Bao, Z. Wang, J. Xie, L. Xu, F. Lei, M. Guan, Y. Zhao, Y. Huang, H. Li, *Chem. Commun.* **2019**, *55*, 3521-3524.
- [S34] A. Jiang, B. Zhang, Z. Li, G. Jin, J. Hao, *Chem. Asian J.* **2018**, *13*, 1438-1446.
- [S35] X. Wang, Y. Chen, J. He, B. Yu, B. Wang, X. Zhang, W. Li, M. Ramadoss, W. Yang, *ACS Appl. Energy Mater.* **2020**, *3*, 1027-1035.
- [S36] J. -F. Qin, J. -H. Lin, T. -S. Chen, D. -P. Liu, J. -Y. Xie, B. -Y. Guo, L. Wang, Y. -M. Chai, B. Dong, *J. Energy Chem.* **2019**, *39*, 182-187.
- [S37] L. Wen, J. Yu, C. Xing, D. Liu, X. Lyu, W. Cai, X. Li, *Nanoscale* **2019**, *11*, 4198-4203.
- [S38] J. Meng, J. Fu, X. Yang, M. Wei, S. Liang, H. -Y. Zang, H. Tan, Y. Wang, Y. Li, *Inorg. Chem. Front.* **2017**, *4*, 1791-1797.
- [S39] A. Kargar, S. Yavuz, T. K. Kim, C. -H. Liu, C. Kuru, C. S. Rustomji, S. Jin, P. R. Bandaru, *ACS Appl. Mater. Interfaces* **2015**, *7*, 17851-17856.
- [S40] C. Xia, Q. Jiang, C. Zhao, M. N. Hedhili, H. N. Alshareef, *Adv. Mater.* **2016**, *28*, 77-85.
- [S41] L. Feng, A. Li, Y. Li, J. Liu, L. Wang, L. Huang, Y. Wang, X. Ge, *ChemPlusChem*, **2017**, *82*, 483-488.
- [S42] X. Zou, A. Goswami, T. Asefa, *J. Am. Chem. Soc.* **2013**, *135*, 17242-17245.
- [S43] X. Yu, M. Zhang, W. Yuan, G. Shi, *J. Mater. Chem. A* **2015**, *3*, 6921-6928.
- [S44] F. Song, X. Hu, *J. Am. Chem. Soc.* **2014**, *136*, 16481-16484.
- [S45] Y. Li, C. Zhao, *ACS Catal.* **2017**, *7*, 2535-2541.
- [S46] C. Dong, X. Yuan, X. Wang, X. Liu, W. Dong, R. Wang, Y. Duan, F. Huang, *J. Mater. Chem. A* **2016**, *4*, 11292-11298.
- [S47] M. Gong, Y. Li, H. Wang, Y. Liang, J. Z. Wu, J. Zhou, J. Wang, T. Regier, F. Wei, H. Dai, *J. Am. Chem. Soc.* **2013**, *135*, 8452-8455.
- [S48] R. Liu, Y. Wang, D. Liu, Y. Zou, S. Wang, *Adv. Mater.* **2017**, *29*, 1701546.
- [S49] N. Han, F. Zhao, Y. Li, *J. Mater. Chem. A* **2015**, *3*, 16348-16353.
- [S50] C. Wang, H. Xu, Y. Wang, H. Shang, L. Jin, F. Ren, T. Song, J. Guo, Y. Du, *Inorg. Chem.* **2020**, *59*, 11814-11822.
- [S51] P. Zhou, X. Lv, D. Xing, F. Ma, Y. Liu, Z. Wang, P. Wang, Z. Zheng, Y. Dai, B. Huang, *Appl. Catal. B: Environ.* **2020**, *263*, 118330.

- [S52] Y. Li, X. Jiang, Z. Miao, J. Tang, Q. Zheng, F. Xie, D. Lin, *ChemCatChem* **2020**, *20*, 917-925.
- [S53] W. Liu, J. Bao, M. Guan, Y. Zhao, J. Lian, J. Qiu, L. Xu, Y. Huang, J. Qian, H. Li, *Dalton Trans.* **2017**, *46*, 8372-8376.
- [S54] L. Hui, Y. Xue, B. Huang, H. Yu, C. Zhang, D. Zhang, D. Jia, Y. Zhao, Y. Li, H. Liu, Y. Li, *Nat. Commun.* **2018**, *9*, 5309.
- [S55] T. Chen, R. Zhang, G. Chen, J. Huang, W. Chen, X. Wang, D. Chen, C. Li, K. Ostrikov, *Catal. Today* **2019**, *337*, 147-154.
- [S56] L. Yu, H. Zhou, J. Sun, F. Qin, D. Luo, L. Xie, F. Yu, J. Bao, Y. Li, Y. Yu, S. Chen, Z. Ren, *Nano Energy* **2017**, *41*, 327-336.
- [S57] B. Zhang, C. Zhu, Z. Wu, E. Stavitski, Y. H. Lui, T. -H. Kim, H. Liu, L. Huang, X. Luan, L. Zhou, K. Jiang, W. Huang, S. Hu, H. Wang, J. S. Francisco, *Nano Lett.* **2020**, *20*, 136-144.
- [S58] L. Yu, H. Zhou, J. Sun, F. Qin, F. Yu, J. Bao, Y. Yu, S. Chen, Z. Ren, *Energy Environ. Sci.* **2017**, *10*, 1820-1827.
- [S59] T. Liu, P. Li, N. Yao, T. Kong, G. Cheng, S. Luo, *Adv. Mater.* **2019**, *31*, 1806672.
- [S60] A. Indra, U. Paik, T. Song, *Angew. Chem. Int. Ed.* **2018**, *57*, 1241-1245.
- [S61] M. Łukaszewski, M. Soszko, A. Czerwiński, *Int. J. Electrochem. Sci.* **2016**, *11*, 4442-4469.
- [S62] S. Anantharaj, S. Kundu, *ACS Energy Lett.* **2019**, *4*, 1260-1264.
- [S63] S. Anantharaj, S. R. Ede, K. Karthick, S. S. Sankar, K. Sangeetha, P. E. Karthik, S. Kundu, *Energy Environ. Sci.* **2018**, *11*, 744-771.